AIAA SciTech Forum
6-10 January 2020, Orlando, FL
AIAA Scitech 2020 Forum

10.2514/6.2020-0574

Reynolds number dependency in supersonic spatially-developing turbulent boundary layers

Guillermo Araya*, Christian Lagares† and Kenneth Jansen ‡

*, † Dept. of Mechanical Eng., University of Puerto Rico at Mayagüez, PR 00681, USA

‡ Dept. of Aerospace Eng. Sciences, University of Colorado at Boulder, CO 80309, USA

Direct Numerical Simulation (DNS) of compressible spatially-developing turbulent boundary layers (SDTBL) is performed at a Mach number of 2.5 and low/high Reynolds numbers over isothermal Zero-Pressure Gradient (ZPG) flat plates. Turbulent inflow information is generated via a dynamic rescaling-recycling approach (J. Fluid Mech., 670, pp. 581-605, 2011), which avoids the use of empirical correlations in the computation of inlet turbulent scales. The range of the low Reynolds number ($Re_{\delta 2}$) case is approximately 400-800, based on the momentum thickness, freestream velocity and wall viscosity. DNS at higher Reynolds numbers ($\sim$ 3,000, about four-fold larger) is also carried out with the purpose of analyzing the effect of Reynolds number on the transport phenomena in the supersonic regime. Additionally, low/high order flow statistics are compared with DNS of an incompressible isothermal ZPG boundary layer at similar low Reynolds numbers and the temperature regarded as a passive scalar. Peaks of turbulence intensities move closer to the wall as the Reynolds number increases in the supersonic flat plate. Furthermore, Reynolds shear stresses depict a much larger "plateau" (constant shear layer) at the highest Reynolds number considered in present study.

Nomenclature

C_f	Skin friction coefficient
δ	Boundary layer thickness at 99% U_∞
R_{δ_2}	Momentum thickness Reynolds number
M_∞	Freestream Mach number
U_∞	Freestream velocity
U^+_{VD}	Van Driest transform velocity in wall units
T_∞	Freestream temperature
T_r	Recovery temperature
T_w	Wall temperature
ν_w	Wall kinematic viscosity
u_τ	Friction velocity
Superscript	
$+$	Wall-Units
$'$	Fluctuations
Subscript	
inl	inlet
rec	recycle
$_{rms}$	Root-Mean Squared

*Assistant Professor, AIAA Senior Member, araya@mailaps.org
†PhD student
‡AIAA Associate Fellow

I. Background

Unsteady spatially-developing turbulent boundary layers (SDTBL) are of utmost importance to a wide range of disciplines and engineering applications, showing a non-homogeneous conditions along the flow direction. In fact, the latter mentioned feature makes SDTBL problematic and burdensome when numerically solved. This arises because of the imperative demand for accurate, realistic and adequate turbulent inflow conditions. Furthermore, the problem becomes harder if the purpose consists on evaluating the flow compressibility influence and turbulent transport phenomena at large Reynolds numbers. In this sense, Direct Numerical Simulation (DNS) may shed important light on the not-well-understood aspects of high speed flows and boundary layer situations (see fig. 1). In the last few decades, the development of more efficient control techniques for the fluid flow and aerodynamic heating in high-speed turbulent boundary layers has led to better flow phenomena understanding, particularly in the near wall region where most of the experimental techniques and turbulence models exhibit serious limitations. Moreover, the dynamics of turbulent structures and instantaneous flow field can be much better analyzed via the extensive spatial information supplied by DNS with millions of "flow and thermal sensors."

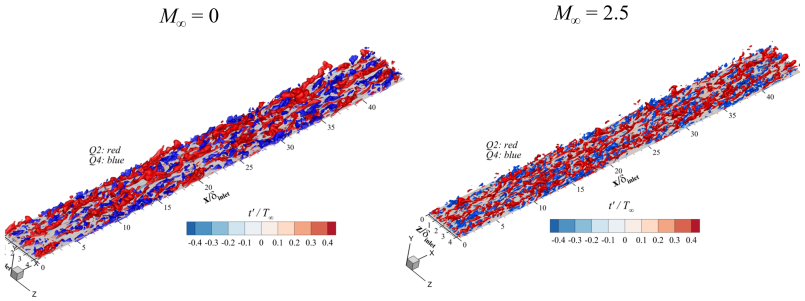

Figure 1. Conditional sampling in incompressible and compressible flows via DNS: Q2 (ejections) and Q4 (sweeps) events.

One of the pioneering DNS of supersonic SDTBL was performed by Guarini *et al.*[20] by resolving an adiabatic wall at a Mach number of $M_\infty = 2.5$ and a Reynolds number, based on the momentum integral thickness and wall viscosity, of $Re_{\delta 2} = 849$. The turbulent inlet information in[20] was generated by making used of the Spalart[22]'s coordinate transformation for incompressible ZPG flow, in which the growth of the boundary layer is so slow that the turbulence can be treated quasi-homogeneous in the streamwise direction. Urbin & Knight[12] and Stolz & Adams[23] evaluated different approaches to the rescaling-recycling method by Lund *et al.*[16] (originally, for incompressible boundary layers) in order to account for compressibility effects. Martin's research group has performed important investigations on supersonic-hypersonic flows by analyzing the effects of Mach number,[8] high enthalpy[9] and initialization[17] on zero-pressure gradient (ZPG) boundary layers, which were performed at low momentum-thickness Reynolds numbers ($Re_{\delta 2} \sim 1600$) or $Re_\tau = \delta u_\tau / \nu_w \sim 500$ in spatial domains with streamwise lengths in the order of 10δ, being δ the inlet boundary layer thickness. Priebe & Martin[19] studied low-frequency unsteadiness by carrying out direct simulations over a 24° compression ramp at Mach 2.9 and $Re_\tau = 340$. They used the recycling-rescaling technique by Xu & Martin[26] and considered an auxiliary domain ($\sim 8.3\delta$ in length with the recycle plane at 7.3δ) to feed turbulent information to a principal domain ($\sim 14.3\delta$ in length) obtaining a mesh with 28 million points in total. Beekman *et al.*[4] assessed the influence of the recycling length and the largest turbulent structures on the recycling technique of[26] by performing a DNS of SDTBL at Mach 2.9 and $Re_\tau \sim 640$ on a large computational domain (about 60-inlet boundary layer thicknesses in streamwise length). Based on Simens *et al.*[21] large eddy evolution time scale definition of δ/u_τ, Beekman *et al.*[4] estimated that a necessary rescaling length should be in the order of $O(12\delta)$ to allow a natural evolution of large scale motions (LSM) before recycling it. They also showed that the recycle plane was nearly disjoint from the most energetic turbulent scales when located at 57δ.

The high computational resources required by DNS in transient predictions of compressible spatially developing turbulent boundary layers (i.e., high-scalable parallel flow solvers) plus the need of efficient turbulent inlet conditions and small physical time steps have certainly prevented the advance of high spatial/temporal resolution numerical simulations. In the present manuscript, we are making use of a dynamic approach to connect the friction velocities at the inlet and recycle stations, which permits to account for the effects of arbitrary Reynolds and Mach numbers. Thus, there is no need of an empirical correlation as in Lund *et al.*,[16] Urbin & Knight[12] and Stolz & Adams.[23] The benefit of the previously described body of work lies in the potential impact to high-speed applied aerodynamics; in fact, comparing results at significantly different

Reynolds numbers can lead to more optimal supersonic vehicle design. The major objective of the present manuscript is to evaluate the Reynolds number dependency of the transport phenomena (momentum and thermal) inside the turbulent boundary layer at the supersonic flow regime.

II. Numerical Methodology

Modeling the physics of turbulent spatially-developing boundary layers by using DNS is arduous, due to the following reasons: i) high mesh resolution required in order to resolve the smallest turbulence scales (Kolmogorov and Batchelor scales), ii) the computational box must be large enough to appropriately resolve the influence of the turbulent "superstructures" (Hutchins & Marusic[13]) located in the outer region of the boundary layer, iii) realistic time-dependent inflow turbulent conditions (instantaneous velocity, temperature and pressure) must be prescribed, Araya *et al.*,[2].[3] As articulated earlier, one of the key aspects on the simulations of unsteady spatially-developing turbulent boundary layers is the prescription of accurate and realistic turbulent inflow information. In this study, we will make use of the inflow generation method devised by Araya *et al.*,[2] which is a modified version of the original rescaling-recycling method by Lund *et al.*[16] A block diagram is shown in fig. 2. The seminal idea of the rescaling-recycling method is to extract the flow solution (mean and fluctuating components of the velocity, thermal and pressure fields) from a downstream plane (called "recycle") and after performing a transformation by means of scaling functions, the transformed profiles are re-injected at the inlet plane, as seen in figure 3. The principal purpose of implementing scaling laws to the flow solution is to convert the streamwise in-homogeneity of the flow into quasi-homogeneous conditions. The Reynolds decomposition is implemented for instantaneous parameters, i.e. a time-averaged plus a fluctuating component:

$$u_i(\mathbf{x},t) = U_i(x,y) + u_i'(\mathbf{x},t) \tag{1}$$

$$t(\mathbf{x},t) = T(x,y) + t'(\mathbf{x},t) \tag{2}$$

$$p(\mathbf{x},t) = P(x,y) + p'(\mathbf{x},t) \tag{3}$$

The turbulent boundary layer is divided into inner and outer zones, where different scaling laws are applied.[2] The projection of flow parameters from the recycle plane to the inlet is performed along constant values of y^+ (inner region) and y/δ (outer region). Figure 3 depicts the schematic of the computational domain in the supersonic regime and at low Reynolds numbers. During the re-scaling process of the flow parameters in the inflow generation methodology,[2] the ratio of the inlet friction velocity to the recycle friction velocity (i.e., $\lambda = u_{\tau,inl}/u_{\tau,rec}$) is required. The friction velocity is defined as $u_\tau = \sqrt{\tau_w/\rho}$, where τ_w is the wall shear stress and ρ is the fluid density. Since the inlet boundary layer thickness must be prescribed according to the predicted inlet Reynolds number, prescribing also the inlet friction velocity would be redundant. To solve this issue, Lund *et al.*,[16] Urbin & Knight[12] and Stolz & Adams[23] used the well-known 1/8-power law that connects the friction velocity to the momentum thickness in zero-pressure gradient flows; thus, $u_{\tau,inl}/u_{\tau,rec} = (\delta_{2,inl}/\delta_{2,rec})^{-1/8}$. The empirical power (-1/8) is strongly affected by the Reynolds number dependency; therefore, we explicitly compute this power, $\gamma_{\delta 2}$, by relating the mean flow solution from a new plane (so-called the "Test" plane, as seen in figure 3) to the solution from the recycle plane as follows:

$$\gamma_{\delta 2} = \frac{ln(u_{\tau,test}/u_{\tau,rec})}{ln(\delta_{2,test}/\delta_{2,rec})}. \tag{4}$$

Figure 4 exhibits a representative time series of the dynamically computed power law exponent $\gamma_{\delta 2}$ computed by Eq. 4 in the supersonic flat plate at high Reynolds numbers as in Table 1. This case was initialized based on an incompressible flow solution. It is observed that $\gamma_{\delta 2}$ fluctuates wildly during the transient stage, and, later tends to the approximate value of -0.1093, which differs in about 12% from the classical empirical value of $-1/8$ (see White[24]). However, this value of $\gamma_{\delta 2}$ is much closer to the empirical value (-0.105) obtained from experiments by Coles, Mabey and Shutts[5,10,11] at a Mach number range of $2.5 < M_\infty < 4.5$ and high Reynolds numbers. Moreover, at low Reynolds numbers the $\gamma_{\delta 2}$ values were -0.083 and -0.081 in the incompressible and supersonic case, respectively. This indicates a negligible effect of compressibility on the $\gamma_{\delta 2}$ exponent in the supersonic regime at low to moderate Reynolds numbers. Once the exponent $\gamma_{\delta 2}$ is obtained from Eq. 4, the values of $u_{\tau,inl}$ and λ can be calculated.

In order to perform the proposed DNS, a highly accurate, very efficient, and highly scalable CFD solver is required. The flow solver PHASTA is an open-source, parallel, hierarchic (2^{nd} to 5^{th} order accurate),

adaptive, stabilized (finite-element) transient analysis tool for the solution of compressible[25] or incompressible flows (Jansen[15]). PHASTA has been extensively validated in a suite of DNS under different external conditions,[2],[1].[7]

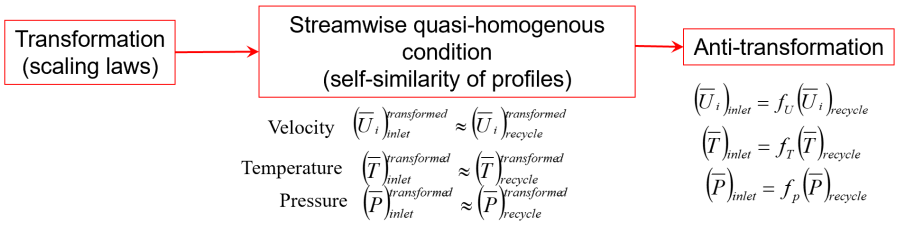

Figure 2. The rescaling-recycling method.

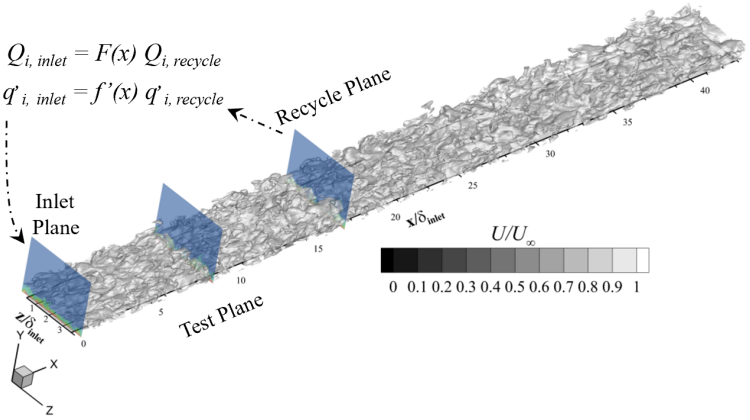

Figure 3. Schematic of the supersonic spatially-developing boundary layer with Inlet, Recycle and Test planes about $43\delta_{inlet}$ of streamwise length.

Boundary Conditions: At the wall, the classical no-slip condition is imposed for all velocity components. Quasi-adiabatic wall condition is assumed for the thermal field. For both compressible flow cases, the ratio T_w/T_∞ is 2.25, where T_w is the wall temperature and T_∞ is the freestream temperature. The T_r/T_∞ ratio is 2.12 for M_∞ equals to 2.5. T_r is the recovery or adiabatic temperature. The lateral boundary conditions are handled via periodicity; whereas, freestream values are prescribed on the top surface.

Table 1 summarizes the characteristics of the proposed three (3) cases: the incompressible case ($M_\infty = 0$) and compressible cases ($M_\infty = 2.5$) at low and high $Re_{\delta 2}$. The Reynolds number range, computational domain dimensions in terms of the inlet boundary layer thickness δ_{inl} (where L_x, L_y and L_z represent the streamwise, wall-normal and spanwise domain length, respectively) and mesh resolution in wall units (Δx^+, Δy^+_{min}, Δy^+_{max}, Δz^+) are also given. For the low Reynolds number cases (i.e., LowReIC and LowReC), the number of mesh points in the streamwise, wall-normal and spanwise direction is 440 × 60 × 80, respectively. These low $Re_{\delta 2}$ cases were run in 96 processors at the Comet supercomputer (SDSC). The high Reynolds number case has the following grid point number: 990 × 250 × 210 (roughly a 52-million point mesh). This case was run in 1200 processors at the Blue Waters supercomputer (NCSA), consuming about 180,000 CPU hours.

Table 1. DNS Cases.

Case	M_∞	$Re_{\delta 2}$	$L_x \times L_y \times L_z$	Δx^+,$\Delta y^+_{min}/\Delta y^+_{max}$, Δz^+
LowReIC	0	306-578	$45\delta_{inl} \times 3.5\delta_{inl} \times 4.3\delta_{inl}$	14.7, 0.2/13, 8
LowReC	2.5	434-816	$43\delta_{inl} \times 3.5\delta_{inl} \times 4.3\delta_{inl}$	15, 0.2/14, 9
HighReC	2.5	2395-3040	$15.2\delta_{inl} \times 3\delta_{inl} \times 3\delta_{inl}$	11.9, 0.4/11, 11

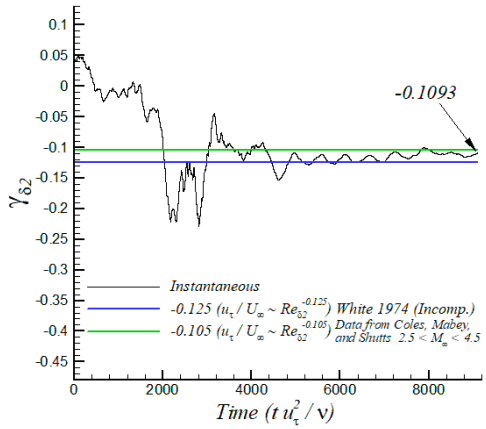

Figure 4. Time-series of the dynamically computed power-law exponent $\gamma_{\delta 2}$ for supersonic flow at high Reynolds numbers.

III. DNS Validation

A thorough validation of the numerical results follows as the consequent analysis and conclusions depend deeply on the validity of the proposed numerical procedure. For the time-averaged streamwise velocity and compressible flow, the Van Driest transform is applied,

$$U_{VD} = \int_0^U \left(\frac{T_w}{T}\right)^{1/2} dU \tag{5}$$

where the integral was numerically computed via a 4-point stencil. The results are seen in Figure 5 where a very good level of collapse in incompressible and compressible profiles is achieved up to $y^+ = 15$ according to the Van Driest's theory. Beyond that point in the buffer region and up to the wake region, a small "gap" is seen between the LowReIC and LowReC cases. A good agreement of present Mach-2.5 case at $Re_{\delta 2} = 655$ is observed with DNS by Guarini *et al.*[20] at slightly higher Reynolds numbers. The high Reynolds number case (HighReC) at $M_\infty = 2.5$ exhibits a significant longer log region ($20 < y^+ < 300$). There is a good agreement with the log law proposed by[14] for a von Karman constant $\kappa = 0.38$ and integration constant $A = 4.1$. More importantly, our HighReC case shows an excellent agreement with experimental data by Mabey and Sawyer[6] at $Re_{\delta 2} = 5{,}970$ and $M_\infty = 2.49$ in the log region.

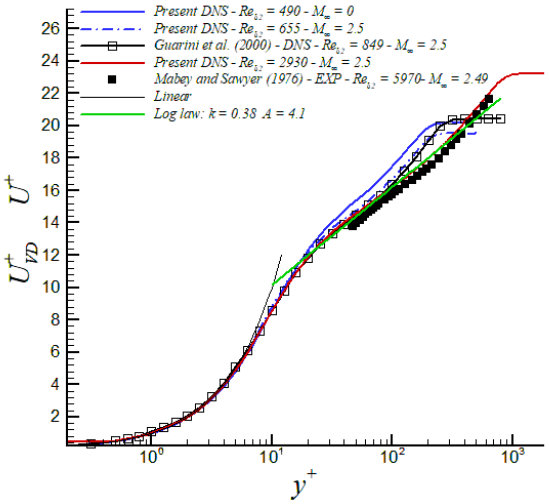

Figure 5. Dimensionless velocity profiles. All compressible profiles are compared using the Van Driest transform.

Turning to the mean static temperature in supersonic flow, the T/T_∞ and U/U_∞ relationship is expressed in terms of the Walz's equation,

$$\frac{T}{T_\infty} = \frac{T_w}{T_\infty} + \frac{T_r - T_w}{T_\infty}\left(\frac{U}{U_\infty}\right) - r\frac{\gamma-1}{2}M_\infty^2\left(\frac{U}{U_\infty}\right)^2 \tag{6}$$

where r is the recovery factor ($= Pr^{1/3}$) and T_r the well known recovery temperature. Figure 6 shows the results for the compressible cases. It can be seen that at low Reynolds number there is an excellent agreement with the Walz's equation. Whereas, for the high Reynolds number case a good agreement is observed in the near wall region at low values of U/U_∞; however, some discrepancies (in the order of 4%) can be seen in the outer region of the boundary layer.

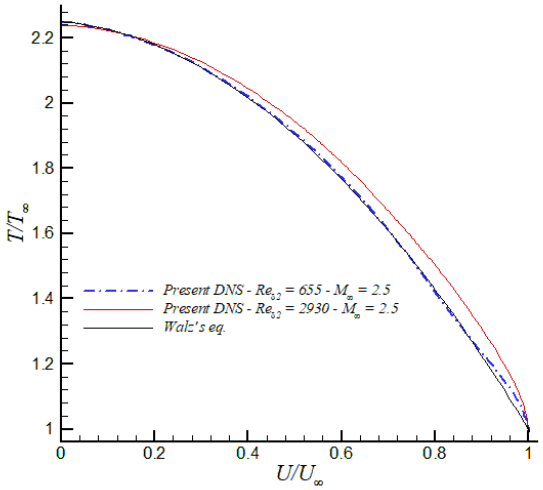

Figure 6. DNS validation through Walz's equation.

The three components of turbulence intensities are plotted in outer-inner scaling in fig. 7 (a). The major Reynolds number effect can be described as a significant displacement of peak values toward the near wall region as $Re_{\delta 2}$ increases. Particularly, in peaks of u'^+_{rms} with $y-$displacements of up to $4\%\delta$. Additionally, the turbulence intensities in the near wall region (i.e., $y/\delta < 0.01$) are greatly enhanced at high Reynolds numbers. By comparing cases at similar low Reynolds numbers (LowReIC vs. LowReC), it is inferred that compressibility effect is manifested as a moderate movement of turbulence intensity peaks closer to the wall. Present DNS results for incompressible flow are in good agreement with Schlatter and Orlu,[18] the observed discrepancies can be attributed to some Reynolds number dependency. Furthermore, the same tendency is observed by the Reynolds shear stresses as seen in Figure 7 (b) where an important influence can be related to a change in the Mach number (compressibility). Our results suggest that increasing the Reynolds number results in a displacement of the peak shear stresses towards the wall region whereas the intensity is lower for a compressible flow when compared to an incompressible flow. Furthermore, as the Reynolds number increases, the constant shear layer strongly grows. As in u'^+_{rms} profiles at high Reynolds number, it can be seen a significant level of (negative) correlation between the streamwise and wall-normal velocity fluctuations in the near wall region for $y/\delta < 0.01$ or high intensities of the Reynolds shear stresses. Profiles of the thermal fluctuations in supersonic flow is depicted in fig. 8. Temperature fluctuations are normalized by local values of the mean temperature. Inner peaks of T'_{rms} displace from $y/\delta \approx 0.1$ in the LowReC case to $y/\delta \approx 0.036$ in the HighReC case.

IV. Reynolds/Mach Number Dependency Assessment

Figure 9 (a) shows iso-surfaces of instantaneous streamwise velocity (extracted at $0.75U_\infty$) for the HighReC case under the supersonic regime. The large hydrodynamic turbulent structures look finer and less organized in supersonic flow, with small but intense "gaps" of high speed fluids in between. This high speed

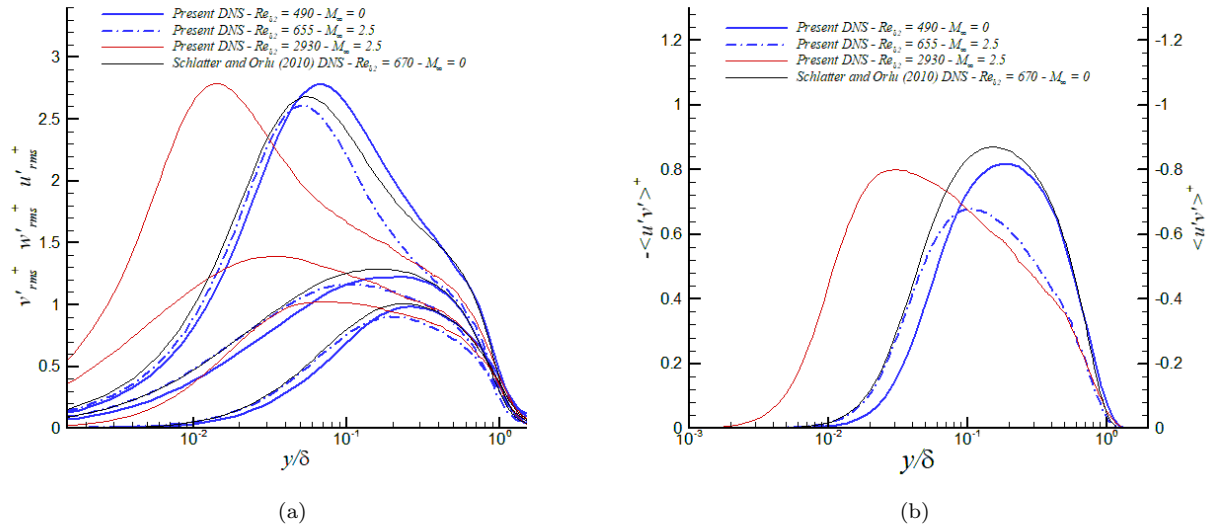

(a) (b)

Figure 7. Effects of Reynolds and Mach numbers on: (a) turbulence intensities, and (b) Reynolds shear stresses.

fluid actually comes from outside the boundary layer (no rotational flow), as observed in figure 9 (b) given by iso-contours of instantaneous streamwise velocity at a cutting XZ plane at 20% of the boundary layer thickness, δ. The skin friction coefficient (C_f) vs. momentum thickness Reynolds numbers ($Re_{\delta 2}$) is plotted in fig. 10 (a). A good agreement with DNS of Guarini *et al.*[20] was obtained in our DNS predictions at similar low Reynolds numbers. On the other hand, the empirical power-law of C_f (i.e., $C_f \sim Re_{\delta 2}^{-0.21}$) obtained from experiments by Coles, Mabey and Shutts[5,10,11] at a Mach number range of $2.5 < M_\infty < 4.5$ (and corrected by the wall to freestream density ratio according to the employed $Re_{\delta 2}$) seems to better fit our high-Reynolds number DNS. The streamwise variation of $Re_{\delta 2}$ along the streamwise direction is exhibited in fig. 10 (b). The steep growth slope of the momentum thickness is evident at large Reynolds numbers, up to five times faster.

Spanwise two-point correlations (TPC) of the streamwise velocity and thermal fluctuations (e.g., R_{uu} and R_{tt}) are plotted in figures 11 and 12 for the incompressible and supersonic case at low Reynolds numbers and at different boundary layer locations ($y^+ = 4$, 15 and 80). In general, a high correlation can be observed between the velocity and thermal field, which is less evident in the supersonic flow case. Furthermore, fluctuations are decorrelated by $z^+ \approx 100$, which indicates the suitability of the selected width of computational box ($L_z^+ \approx 700$). Thus, several low/high speed streaks can be captured. The spanwise spacing between velocity/thermal streaks significantly augments as one moves further from the wall, from $\lambda^+ \approx 100$ in the linear viscous layer to $\lambda^+ \approx 200$ in the log region at $y^+ = 80$. Thermal streaks are separated by a longer distance in this zone, specially in the supersonic case.

Iso-contours of R_{uu} are shown in fig. 13 for a plane YZ for the incompressible and supersonic case at low Reynolds numbers and different vertical locations y^+. Overall, iso-contours of R_{uu} look very similar in both flow regimes; however, they seem "more packed or wrapped" in the outer region at $M_\infty = 2.5$. A similar conclusion can be drawn for two-point correlations of thermal fluctuations R_{tt} in figure 14.

V. Conclusions

Direct simulations of supersonic turbulent flow over a quasi-adiabatic flat plate is carried out at high Reynolds numbers. In addition, a low Reynolds number case and incompressible case have been considered with the purpose of assessing Reynolds and Mach number dependency on flow parameters. When outer units are considered in the wall normal direction, i.e. y/δ, peaks of turbulence intensities move closer to the wall as the Reynolds number increases. Furthermore, Reynolds shear stresses depict a much larger "plateau"

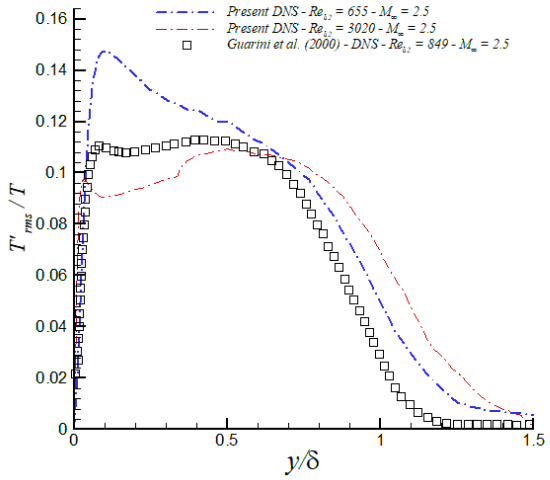

Figure 8. Thermal fluctuations in outer units.

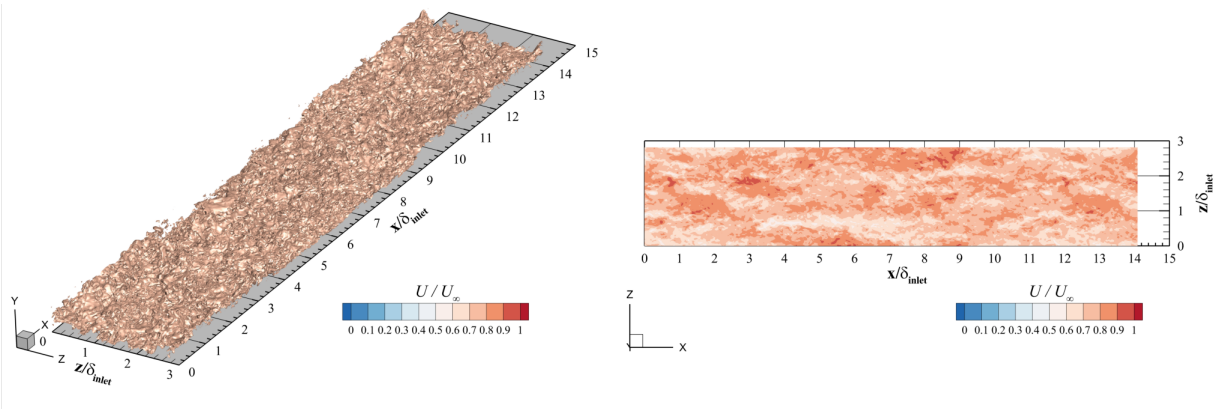

(a) (b)

Figure 9. Iso-surfaces of instantaneous streamwise velocity ($0.75U_\infty$): (a) isometric view, and (b) plane XZ at y/δ =0.2.

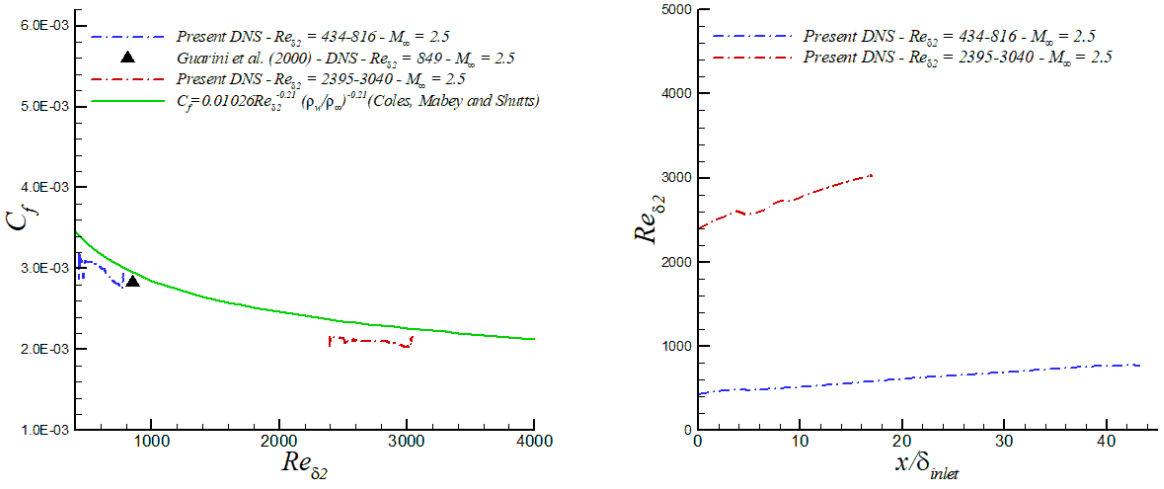

(a) (b)

Figure 10. Effect of Reynolds numbers on (a) C_f, and (b) momentum thickness.

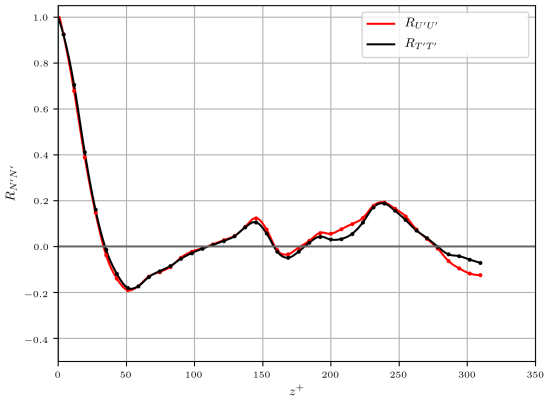

(a) $y^+ = 4$

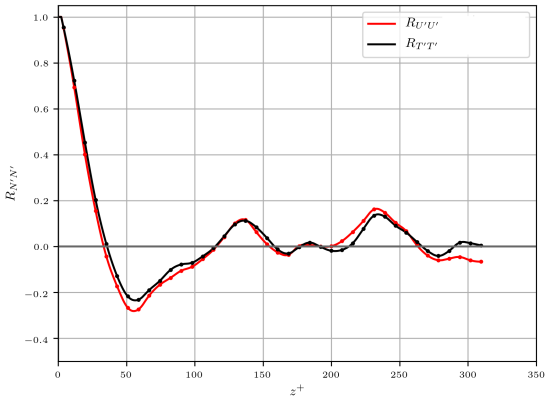

(b) $y^+ = 15$

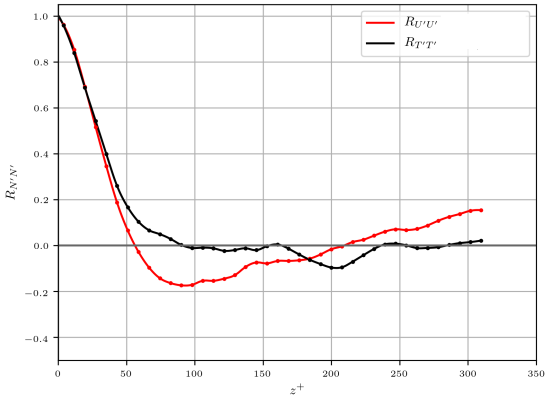

(c) $y^+ = 80$

Figure 11. Two-Point Correlations at Mach = 0.0 (LowReIC).

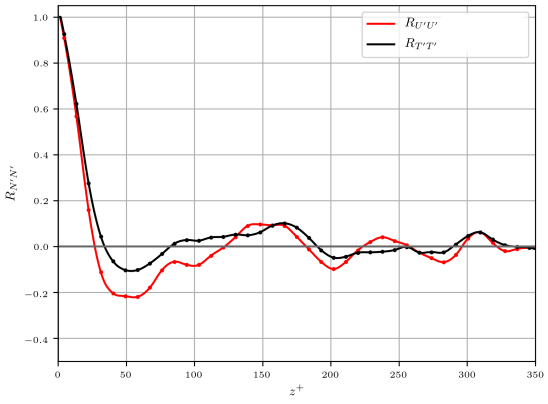

(a) $y^+ = 4$

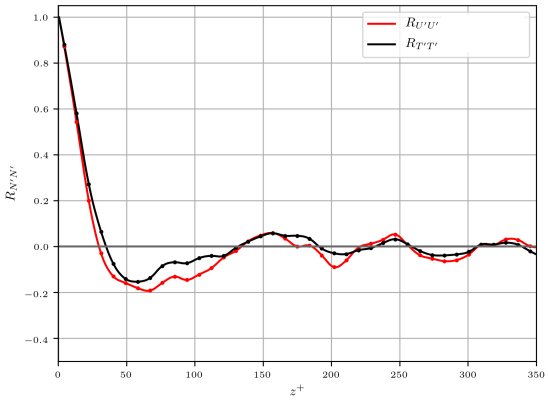

(b) $y^+ = 15$

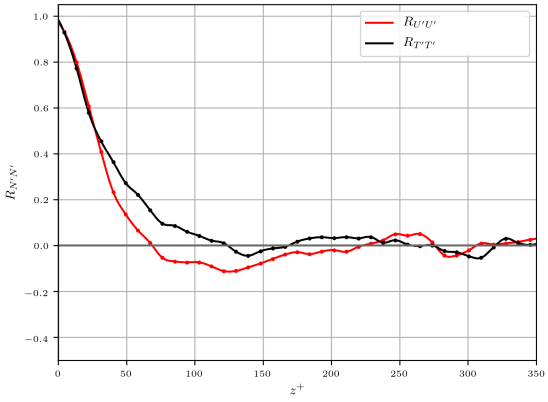

(c) $y^+ = 80$

Figure 12. Two-Point Correlations at Mach = 2.5 (LowReC).

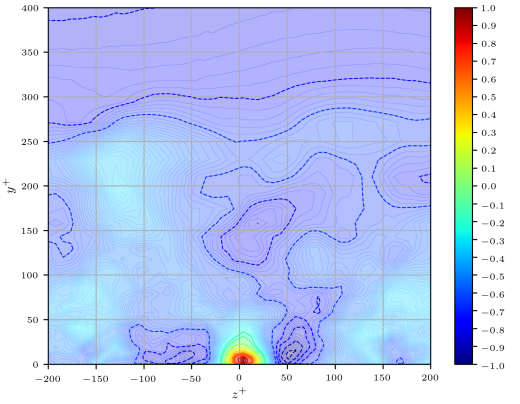

(a) $M_\infty = 0$, $y^+ = 4$

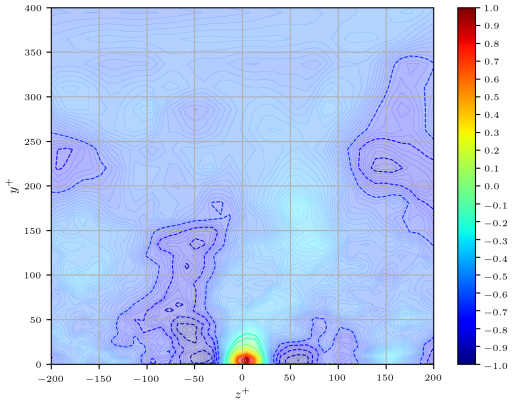

(b) $M_\infty = 2.5$, $y^+ = 4$

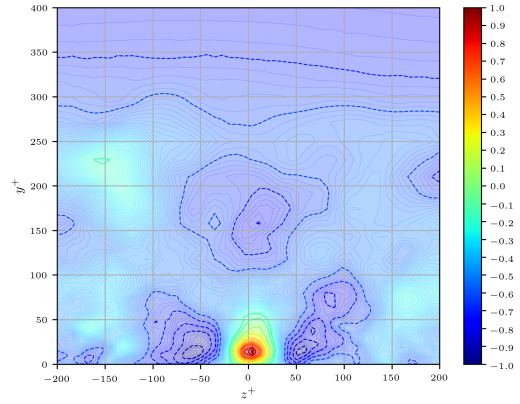

(c) $M_\infty = 0$, $y^+ = 15$

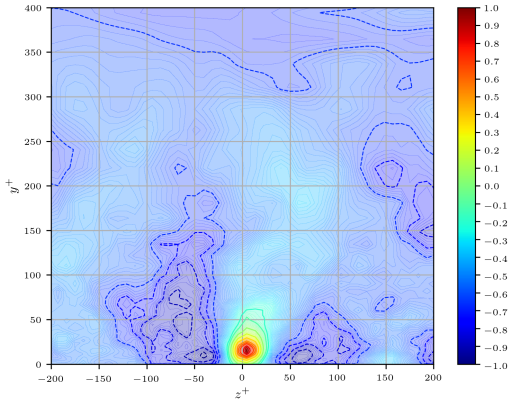

(d) $M_\infty = 2.5$, $y^+ = 15$

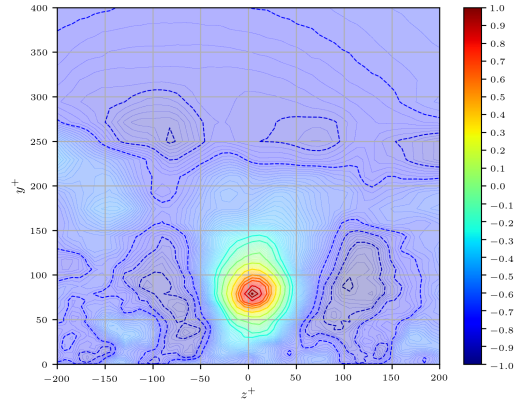

(e) $M_\infty = 0$, $y^+ = 80$

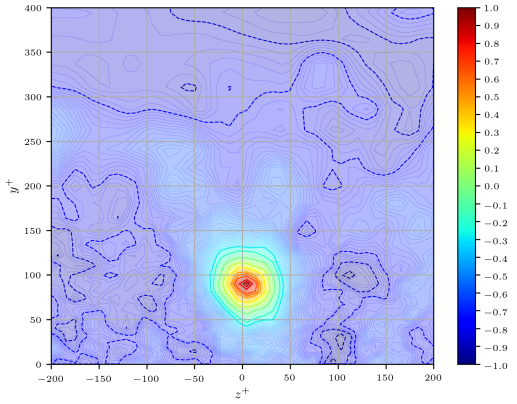

(f) $M_\infty = 2.5$, $y^+ = 80$

Figure 13. Two-point correlations of streamwise velocity fluctuations, R_{uu}.

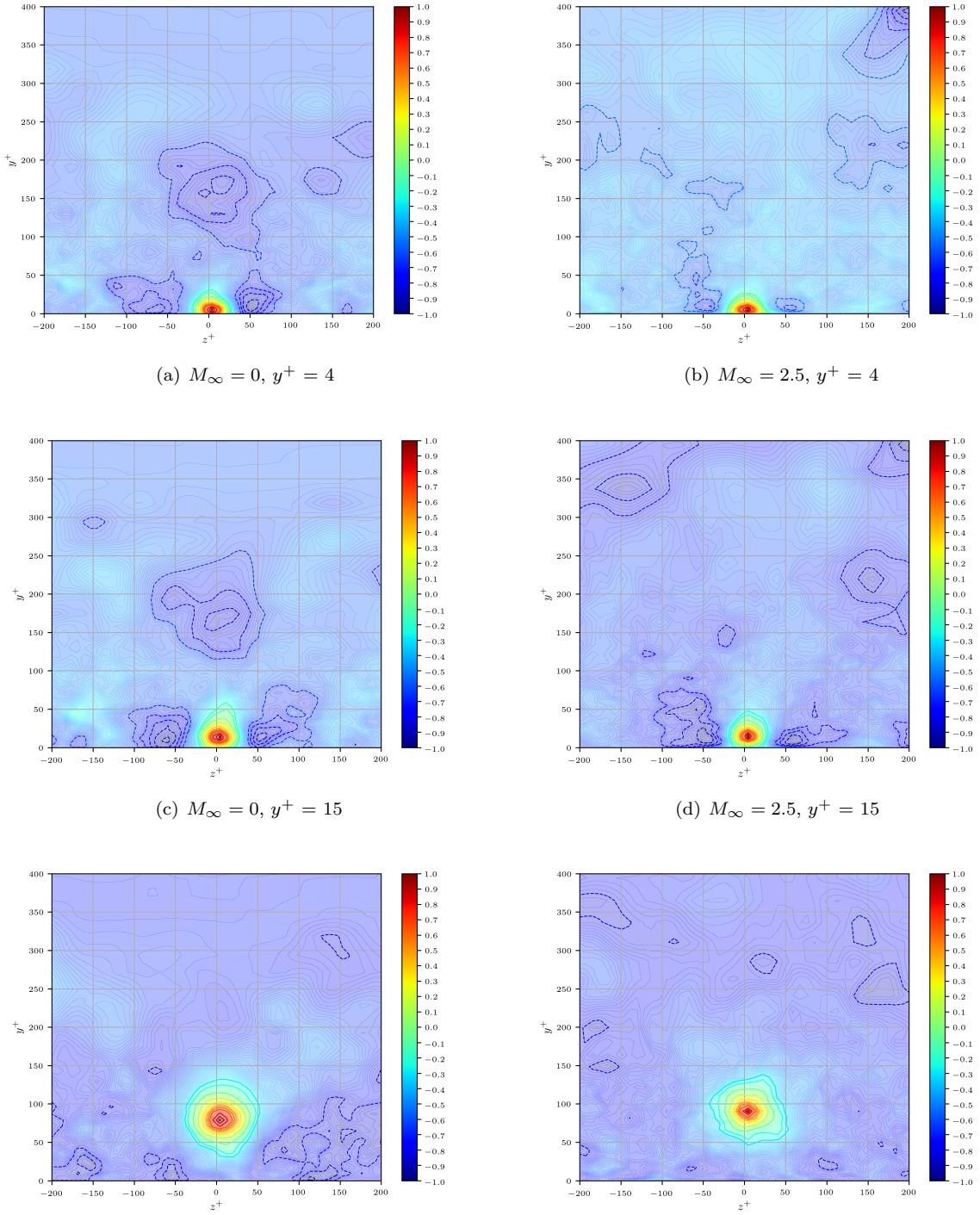

(a) $M_\infty = 0$, $y^+ = 4$

(b) $M_\infty = 2.5$, $y^+ = 4$

(c) $M_\infty = 0$, $y^+ = 15$

(d) $M_\infty = 2.5$, $y^+ = 15$

(e) $M_\infty = 0$, $y^+ = 80$

(f) $M_\infty = 2.5$, $y^+ = 80$

Figure 14. Two-point correlations of thermal fluctuations, R_{tt}.

(constant shear layer) at the highest Reynolds number considered in present study. It is observed a high spatial correlation between the streamwise velocity (u') and temperature (t') fluctuations, particularly in the viscous and buffer layer in the compressible flow regime.

VI. Acknowledgment

This material is based upon work supported by the Air Force Office of Scientific Research under award number FA9550-17-1-0051. GA acknowledges NSF Grant #1847241. Computational resources are supplied by XSEDE project #TG-CTS170006 and a Broadening Participation Allocation at Blue Waters.

References

[1]G. Araya, C. Castillo, and F. Hussain. The log behaviour of the Reynolds shear stress in accelerating turbulent boundary layers. *Journal of Fluid Mechanics*, 775:189–200, 2015.

[2]G. Araya, L. Castillo, C. Meneveau, and K. Jansen. A dynamic multi-scale approach for turbulent inflow boundary conditions in spatially evolving flows. *Journal of Fluid Mechanics*, 670:518–605, 2011.

[3]G. Araya, C. Lagares, and K.E. Jansen. Direct simulation of a Mach-5 turbulent spatially-developing boundary layer. *49^{th} AIAA Fluid Dynamics Conference, AIAA AVIATION Forum, (AIAA 3131876) 17 - 21 June, Dallas, TX*, 2019.

[4]I. Beekman, S. Priebe, Y.C. Kan, and M. P. Martin. Dns of a large-domain, mach 3 turbulent boundary layer: turbulence structure. In *49th AIAA Aerospace Sciences Meeting*, pages 2011–753. AIAA, 2011.

[5]D. Coles. Measurement of turbulent friction on a smooth flat plate in supersonic flow. *J. Aeronaut. Sci.*, 7, 1954.

[6]D. Mabey and W. Sawyer. Experimental studies of the boundary layer on a flat plate at mach numbers from 2.5 to 4.5. *Aerodynamics Department, R.A.E., Bedford.*, Reports and Memoranda No. 3784, 1976.

[7]A. Doosttalab, G. Araya, J. Newman, R. Adrian, K. Jansen, and L. Castillo. Effect of small roughness elements on thermal statistics of a turbulent boundary layer at moderate Reynolds number. *Journal of Fluid Mechanics*, 787:84–115, 2015.

[8]Duan, L. and Beekman, I. and Martin, M. P. Direct numerical simulation of hypersonic turbulent boundary layers. part 3. effect of mach number. *Journal of Fluid Mechanics*, 672:245–267, 2011.

[9]Duan, L. and Martin, M. P. Direct numerical simulation of hypersonic turbulent boundary layers. part 4. effect of high enthalpy. *Journal of Fluid Mechanics*, 684:25–59, 2011.

[10]H. Fernholz and P. Finley. A critical compilation of compressible turbulent boundary layer data. *Technical Report AGARDograph, AGARD*, 223, 1977.

[11]H. Fernholz and P. Finley. A further compilation of compressible boundary layer data with a survey of turbulence data. *Technical Report AGARDograph, AGARD*, 263, 1981.

[12]G. Urbin and D. Knight. Large-Eddy Simulation of a supersonic boundary layer using an unstructured grid. *AIAA Journal*, 39(7):1288–1295, 2001.

[13]N. Hutchins and Ivan Marusic. Evidence of very long meandering features in the logarithmic region of turbulent boundary layers. *Journal of Fluid Mechanics*, 579:1–28, 2007.

[14]J. Osterlund and A. Johansson and H. Nagib and M. Hites. A note on the overlap region in turbulent boundary layers. *Phys. Fluids*, 12:1, 2000.

[15]K. E. Jansen. A stabilized finite element method for computing turbulence. *Comp. Meth. Appl. Mech. Engng.*, 174:299–317, 1999.

[16]T.S. Lund, X. Wu, and K.D. Squires. Generation of turbulent inflow data for spatially-developing boundary layer simulations. *Journal of Computational Physics*, 140(2):233–258, 1998.

[17]Martin, M. P. Direct numerical simulation of hypersonic turbulent boundary layers. part 1. initialization and comparison with experiments. *Journal of Fluid Mechanics*, 570:347–364, 2007.

[18]P. Schlatter and R. Orlu. Assessment of direct numerical simulation data of turbulent boundary layers. *Journal of Fluid Mechanics*, 659:116–126, 2010.

[19]Priebe, S. and Martin, M. P. Low-frequency unsteadiness in shock wave-turbulent boundary layer interaction. *Journal of Fluid Mechanics*, 699:1–49, 2012.

[20]S. Guarini and R. Moser and K. Shariff and A. Wray. Direct numerical simulation of a supersonic turbulent boundary layer at mach 2.5. *Journal of Fluid Mechanics*, 414:1–33, 2000.

[21]J. Simens, M. amd Jimenez, S. Hoyas, , and Y. Mizuno. A high-resolution code for turbulent boundary layers. *J. of Comp. Physics*, 228:4218–4231, 2009.

[22]P.R. Spalart. Direct simulation of a turbulent boundary layer up to $Re_\theta = 1410$. *Journal of Fluid Mechanics*, 187:61–98, 1988.

[23]S. Stolz and N. Adams. Large-eddy simulation of high-Reynolds-number supersonic boundary layers using the approximate deconvolution model and a rescaling and recycling technique. *Physics of Fluids*, 15(8):2398–2412, 2003.

[24]F. M. White. *Viscous Fluid Flow.* McGraw-Hill Mechanical Engineering, New York, 2006.

[25]C. H. Whiting, K. E. Jansen, and S. Dey. Hierarchical basis in stabilized finite element methods for compressible flows. *Comp. Meth. Appl. Mech. Engng.*, 192(47-48):5167–5185, 2003.

[26]S. Xu and M. P. Martin. Assessment of inflow boundary conditions for compressible turbulent boundary layers. *Physics of Fluids*, 16(7):2623–2639, 2004.